Research article

SURFACE and INTERFACE ANALYSIS

Received: 6 November 2012 Revised: 28 November 2012 Accepted: 28 November 2012 Published online in Wiley Online Library: 18 December 2012

(wileyonlinelibrary.com) DOI 10.1002/sia.5202

Laser surface treatment of high-speed tool steel (AISI M2)

B. S. Yilbas,[a]* F. Patel[b] and C. Karatas[c]

High-speed tool steel (AISI M2) surface is pre-prepared to form a thin carbon film containing 5% B_4C particles prior to laser treatment process. Morphological and metallurgical changes are examined in the treated layer using electron microscope, energy dispersive spectroscopy, and X-ray diffraction. The microhardness and the residual stress formed at the treated surfaces are measured for samples with and without B_4C particles. It is found that the micro-stresses formed in the neighborhood of B_4C particles at the treated surface contributed to the microhardness enhancement at the surface. This is associated with the mismatch of thermal expansion coefficients between B_4C particles and the base alloy. The nitride phases are formed at the treated surface, which also contribute to the microhardness increase at the surface. Copyright © 2012 John Wiley & Sons, Ltd.

Keywords: laser; surface treatment; high-speed tool steel; B_4C

Introduction

High-speed tool steels have superior high temperature properties, and they are widely used in tooling industry. The alloy composition can be modified to improve the microhardness through forming dense and carbide rich layer in the surface region. One of the methods to modify the composition of the alloy surface is to introduce hard particle imbedding in the surface region via using laser controlled melting technique. Laser control melting provides fast processing, precision of operation, and local treatment, and the hard particle injection improves further surface hardness of the treated alloy. However, high stress levels are formed in the treated region due to the high cooling rates at the surface and mismatch between the thermal expansion coefficients and the density of the base alloy and the hard particles. This, in turn, limits the practical application of the treated surface. The influence of TiC particles on the metallurgical and morphological changes in the laser-treated layer of steel was investigated previously.[1] The mismatch between the properties of hard particles and the parent modifies the microstructure and thermal induced micro-stress levels in the treated layer. Moreover, introducing the hard particles with relatively lower melting temperature, thermal conductivity, and density than TiC particles, such as B_4C, may improve the surface microhardness and residual stress levels in the laser-treated layer. Consequently, investigation of the morphological, metallurgical changes, surface microhardness, and residual stress developed in the laser-treated layer due to presence of B_4C particles becomes essential.

Laser surface melting of high-speed tool steel was studied by Bonek *et al.*[2] They showed that laser surface melting modified the microstructure in the treated layer and improved the properties at the surface. Laser beam interaction with steel matrix surface nano-composites were investigated by Verezub *et al.*[3] Their findings revealed that nanosized (Fe, W)6C particles precipitated during the subsequent heating from an oversaturated steel matrix. Laser surface treatment of steel surface in association with polishing was examined by Guo.[4] He showed that the influence of the laser pulse federate was more prominent than that of other parameters on the topology of a laser polished surface. Laser surface treatment of pearlitic rail steel for wear testing was carried out by Shariff *et al.*[5] They indicated that microhardness of the laser-treated surface was increased notably and wear resistance of the resulting surface improved significantly. Laser surface modification of zirconia-coated steel surface was studied by Shankar and Mudali.[6] They demonstrated that microstructural inhomogeneities like pores and voids were eliminated in the laser-treated layer, and distinct interface separating fine and coarse grains were observed at all laser scanning speeds. Microstructure and wear properties of laser processed amorphous matrix coatings were investigated by Li *et al.*[7] They showed that wear resistance of the laser-treated surface increased significantly. Characterization study for laser-deposited AISI 316 reinforced ceramic was carried out by Betts *et al.*[8] They indicated that laser re-melted tungsten carbide blended steel powder resulted in improved wear and corrosion resistance. Microstructure and wear properties of laser clad iron-based amorphous composite coatings were examined by Zhu *et al.*[9] Their findings revealed that laser-treated coatings had higher hardness and better wear property than the base substrate.

Laser treatment of high-speed tool steel was investigated previously,[1,10,11] and the main emphasis was to introduce gas assisted nitriding at the alloy surface. Although the microhardness at the laser surface increased considerably, the surface hardness can be further improved through the insertion of hard particles, such as carbides, during the laser control melting of the surface.

* *Correspondence to: B. S. Yilbas, ME Department, King Fahd University of Petroleum and Minerals, Dhahran, Saudi Arabia.*
E-mail: bsyilbas@kfupm.edu.sa

a *ME Department, King Fahd University of Petroleum and Minerals, Dhahran, Saudi Arabia*

b *ME Department, King Fahd University of Petroleum and Minerals, Dhahran, Saudi Arabia*

c *Engineering College, Hacettepe University, Turkey*

Consequently, in the present study laser treatment of pre-prepared high-speed tool steel (ASTM A600) surface is carried out. A thin carbon film accommodating 5% of B_4C particles is formed at the alloy surface prior to the laser treatment process. Morphological and metallurgical changes in the treated layer are examined using optical microscope, scanning electron microscope (SEM), energy dispersive spectroscopy (EDS), and X-ray diffraction (XRD). The residual stress developed at the surface is determined incorporating the XRD technique.

Experimental

The CO_2 laser (LC-ALPHAIII) delivering nominal output power of 2 kW was used to irradiate the workpiece surface. The laser parameters were selected after conducting the several surface treatment tests; in which case, the laser parameters resulting in low asperities and crack-free surface are selected to carry out the experiments. Nitrogen assisting gas emerging from the conical nozzle and co-axially with the laser beam was used. High-speed tool steel (AISI M2) samples in $15\times10\times3$ mm^3 sizes were used as workpieces. The carbon film containing uniformly distributed 5% B_4C was formed at the workpiece surface prior to the laser treatment process. The method applied for the formation of carbon film is similar to that presented in the previous study.[12] The laser beam was scanned surface according to the parameters given in Table 1.

Jeol 6460 electron microscopy is used for SEM examinations, and Bruker D8 Advanced having Cu-Kα radiation is used for XRD analysis of the laser-treated surfaces. Microphotonics digital microhardness tester (MP-100TC) was used to obtain microhardness at the surface of the laser-treated layer. The residual stress (σ) is obtained using the XRD technique.[13] The bcc ferrite steel peak at (211) planes takes place at $2\theta = 88.3^{\circ}$ with the inter-planer spacing of 0.11709 nm. The linear dependence of d(211) results in the slope of -3.582×10^{-13} m and the intercept of 1.17×10^{-10} m as shown in Fig. 1. The slope of the curve indicates that the residual stress is compressive and the residual stress determined is of the order of -560 ± 20 MPa.

Results and discussion

Laser melting of high-speed tool steel (AISI M2) alloy is carried out, and the alloy surface is treated to form a thin carbon film containing 5% B_4C particles prior to laser treatment process. Morphological and metallurgical changes in the treated layer are examined using the analytical tools. The residual stress at the surface is obtained incorporating the XRD technique.

Figure 2 shows optical photograph and SEM micrographs of laser-scanned tracks at the surface. It is evident from the SEM micrographs that tracks formed during laser scanning are parallel at the surface. Since the laser-irradiated energy is delivered in repetitive pulses, overlapping of the laser spots at the surface is visible. The pulsing frequency of the laser output energy is on

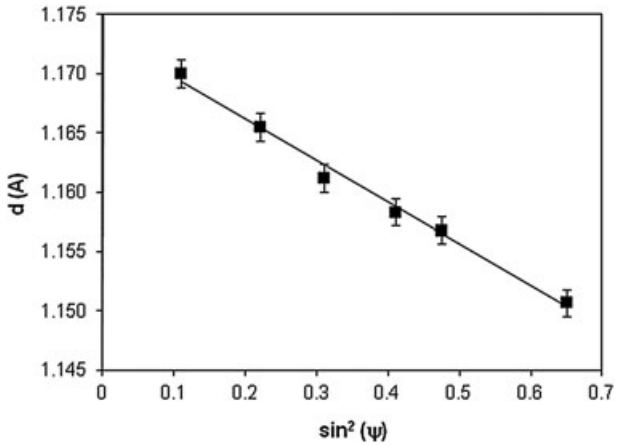

Figure 1. Linear variation of d(211) with $\sin^2(\psi)$ for the laser-treated surface.

the order of 1500 Hz. This results in continuous melting of the substrate material at the surface. The overlapping ratio of the spots is about 75%. Moreover, the laser output power intensity is set such that evaporation at the surface is avoided. This, in-turn, lowers the asperities and reduces the roughness of the treated surface, since laser-produced cavities, due to evaporation, enhances the surface roughness. Although the cooling rates at the surface is high due to convection effect of the assisting gas, no major crack or crack network is observed at the surface. In addition, mismatch of thermal expansion coefficients of B_4C particles and the base alloy causes micro-stress development in the close boundaries of B_4C particles. This contributes to overall stress development in the treated layer. However, no crack is observed in the neighborhood of the particles. This indicates that the stress level is not high enough to trigger the crack initiation and the propagation in this region. It should be noted that initially formed laser-scanned tracks act like a heat source while generating annealing effect on the treated surface. This suppresses the attainment of high stress levels in the treated layer. Moreover, the close examination of SEM micrograph reveals that partially embedded B_4C particles are evident at the surface. Although the surface temperature is above the melting temperature of the base alloy, it is not high enough to cause dissolution or total immersion of all B_4C particles at the surface.

Figure 3 shows SEM micrographs of the cross section of the laser-treated layer. The treated layer cross section is free from defects such as large size cracks and voids. The treated layer extends almost 50 μm below the surface having the uniform thickness along the cross section. Four regions can be distinguishable across the cross section of the treated layer. The first region consists of fine size grains and dense structure. This is attributed to the high cooling rates from the surface because of the convection effect of the assisting gas. In addition, the presence of B_4C particles is evident in this region. Although thermal expansion coefficient difference between B_4C and the

Table 1. Laser heating conditions used in the experiment

Scanning speed (cm/s) (mm/min)	Power (W)	Frequency (Hz)	Nozzle gap (mm)	Nozzle diameter (mm)	Focus setting (mm)	N_2 Pressure (kPa)
10	85	1000	1.5	1.5	127	600

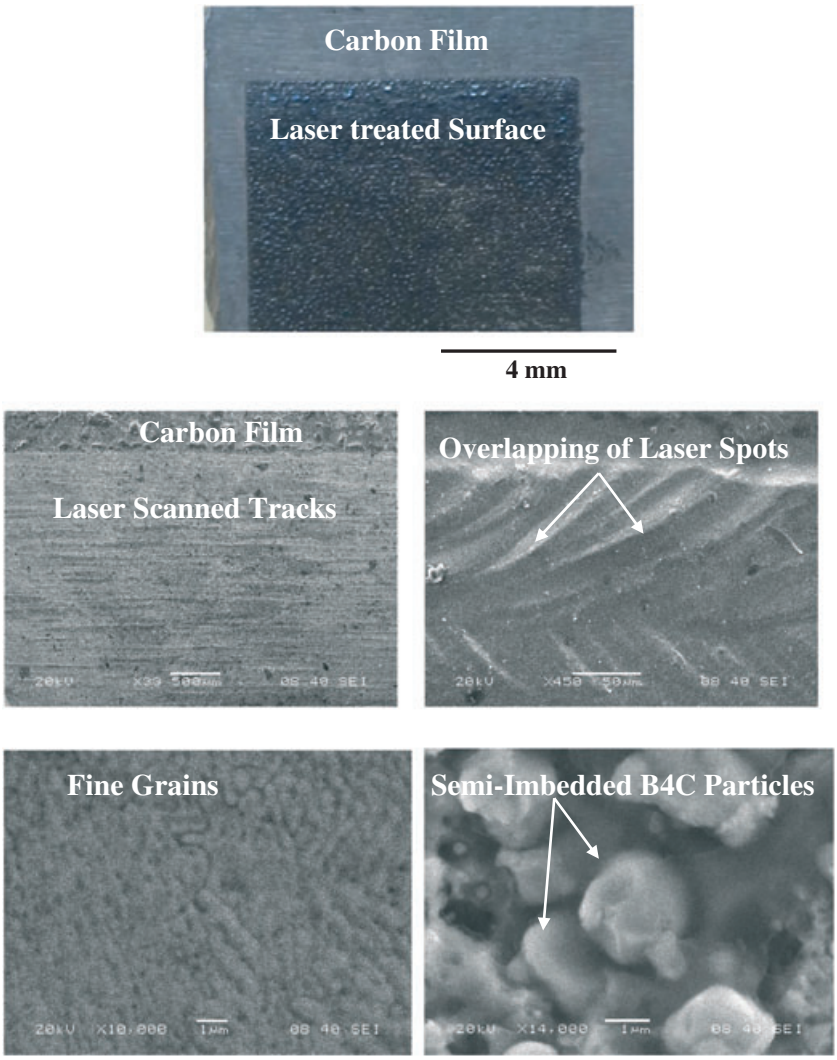

Figure 2. Optical photograph and SEM micrographs of laser-treated surface.

alloy causes the development of micro-stresses in the close region of B_4C particles, no evidence of stress induced micro-crack is observed in the dense layer. The volume shrinkage due to the dense layer contributes to the stress level in this region. The self annealing effect of the initially formed tracks is responsible stress relaxation in this region; in which case, micro-crack formation around B_4C particles is avoided. The microstructure consists of phase mixture of ferrite and carbides transforms into martensite and very fine carbides in the vicinity of the dense layer occur due to the high cooling rates from the surface. In this case, rapid quenching in the surface region contributes to the refinement of carbides in this region. The feathery-like structure is observed in the second region, which is associated with the nitride formation in this region. Therefore, nitrogen diffusion from the surface along the grain boundaries is responsible for the formation of the feathery-like structures in this region. Since the nitride phase formation is related with the exothermic reactions, the heat generated in this region contributes to the self-annealing effect occurring in the surface region. Moreover, fine dendrites are also formed in the second region. The dendrites are martensite with certain amount of retained austenite due to high cooling rates. As the depth below the surface increases, the dendrite size increases because of slower cooling rates as compared to that corresponding to the surface vicinity. Due to the slow cooling rate, primary austenite partially transforms into martensite in this region. In the third region, cellular structure is observed, which is associated with the relatively slower cooling rates than that of the second region. The heat conducted from the first and second region towards the third region results in homogenized austenized microstructure in this region. The neighborhood of the heat-affected zone corresponds to the fourth region. The size of the cells become large, and they deform due to slow cooling rates in this region. The demarcation line between the laser-treated layer and the base alloy is visible in this region.

Figure 4 shows X-ray diffractogram for the laser-treated surface. The peaks of nitride compounds at the treated surface are present. This reveals that the use of high pressure assisting gas causes the formation of the nitride compounds at the surface. In addition, presence of Fe_4N indicates the nitrogen diffusion through grain boundaries while resulting in feathery-like structures in the vicinity of the surface. Fe_3 (N, C) peak is observed in the X-ray diffractogram. The formation of carbon film prior to laser treatment process is attributed to the formation of Fe_3(N, C) phase. In addition, B_4F and CrN peaks are related to the presence of partially dissolved B_4C particles and chromium nitride phase formation at the surface. Table 2 gives the EDS data

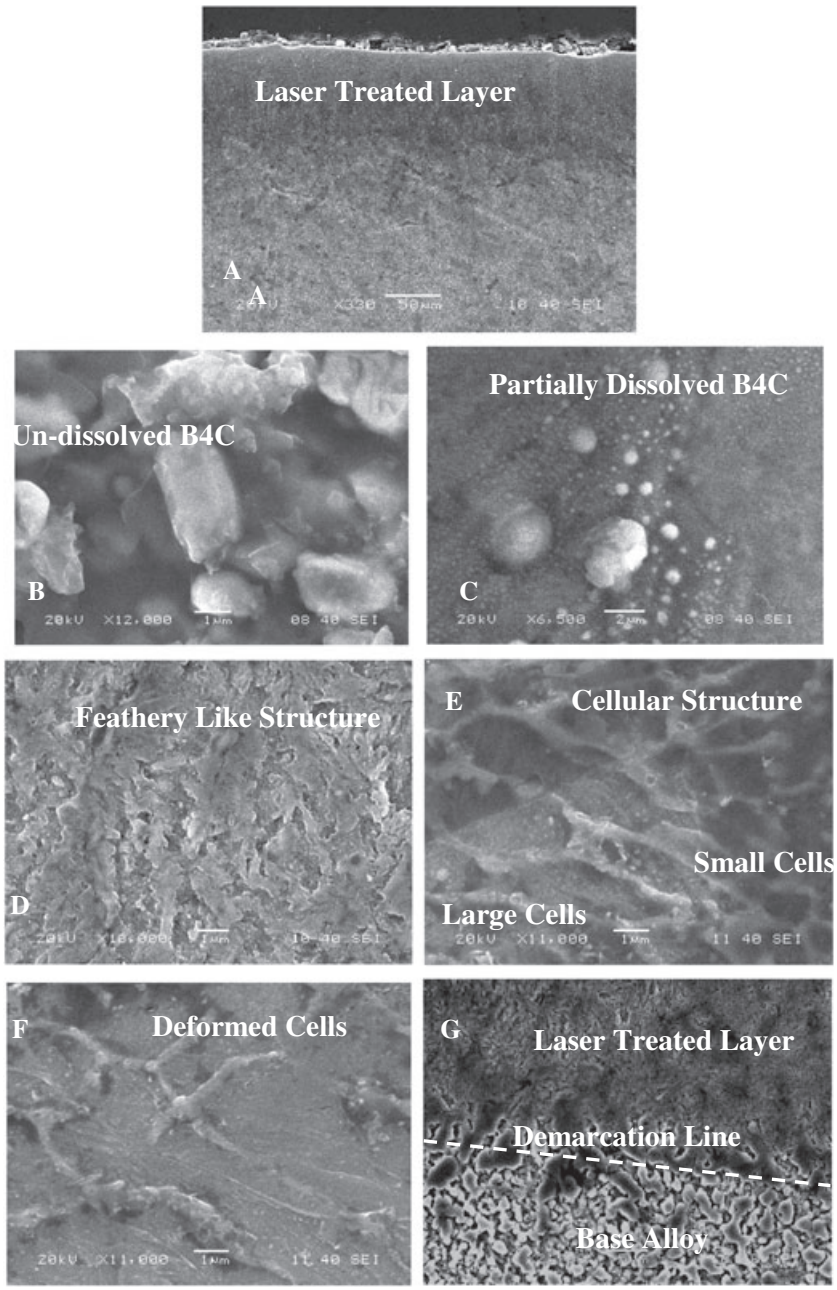

Figure 3. SEM micrographs of the cross section of laser-treated layer: A) Laser-Treated Layer, B) Un-dissolved B4C particles in dense layer, C) Partially dissolved B4C Particles in dense layer, D) Feathery-like structure, E) Cellular structure, F) Deformed cells, G) Demarcation line.

corresponding to the treated surface, while Fig. 5 shows the locations of the spectrums at the surface. Elemental composition of the alloy remains almost uniform at the treated surface. Although the quantification of light elements, such as nitrogen, involves with error, the presence of nitrogen is evident from the EDS data. Table 3 gives the microhardness of the treated surface with and without presence of B_4C particles and the residual stress formed at the surface vicinity for the laser-treated surface with and without presence of B_4C particles. Laser treatment improves microhardness significantly at the surface, which is more pronounced for the treated surface with presence of B_4C particles. In addition, B_4C particles in the treated layer increase the residual stress. The increase in microhardness and residual stress due to presence of B_4C particles is associated with the micro-stress developed in the vicinity of B_4C particles due to the mismatch of thermal expansion coefficients between the particles and the base alloy. In general, enhancement of microhardness at the treated surface is attributed to the followings: (i) formation of dense layer with fine grains at the surface, (ii) nitride phases formed at the surface due to the use of high pressure nitrogen as an assisting gas, and (iii) micro-stresses formed in the neighborhood of B_4C particles.

Conclusion

Laser treatment of high-speed tool steel (AISI M2) surface is carried out and the metallurgical and the morphological changes

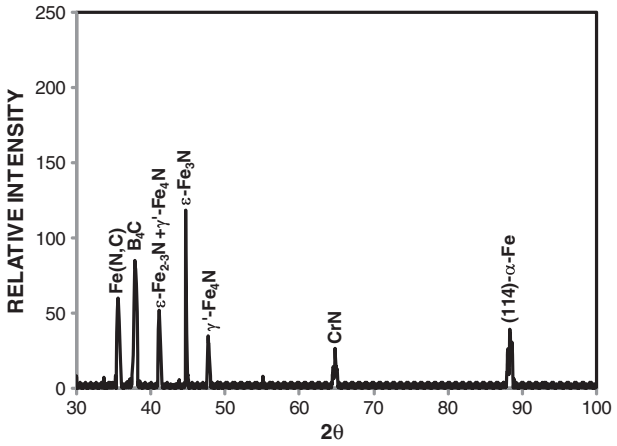

Figure 4. X-ray diffractogram of laser-treated surface.

Table 2. EDS data for laser-treated surface (wt%)

Spectrum	N	B	V	Cr	Mo	W	Fe
Spectrum 1	6.1	5.0	2.1	4.1	5.0	6.1	Balance
Spectrum 2	5.5	4.8	2.0	4.1	4.9	5.9	Balance
Spectrum 3	6.3	4.9	1.9	4.2	5.0	6.4	Balance
Spectrum 4	5.4	5.0	1.7	4.0	5.0	6.0	Balance

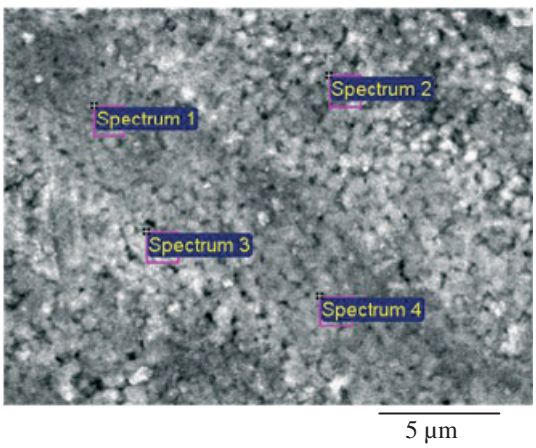

Figure 5. SEM micrograph of the laser-treated surface and the locations of spectrums for the EDS data given in Table 2.

Table 3. Microhardness and residual stress obtained from XRD Technique for the laser-treated and untreated surfaces

	Hardness (HV)	Residual stress (MPa)
As received	700±25	-
Laser nitrided	1050±25	440±15
Laser-treated and B_4C	1350±30	560±20

in the treated layer are examined. A carbon film containing 5% B_4C particles is formed at the workpiece surface prior to the laser treatment process. The optimum laser parameters are selected in the treatment process; in which case, surface asperities and defects in the treated layer are avoided. Although the thermal expansion coefficients of B_4C particles and the base alloy are different, no micro-cracks or crack network is observed in the vicinity of the particles in the treated layer. The laser-treated layer extends uniformly below the surface. The thickness of the treated layer is about 50 μm, which consists of four distinct regions. The dense layer with fine grains are formed at the surface, which is associated with the high cooling rates from the surface due to convection effect of the assisting gas. Although the volume shrinkage contributes to the stress levels in the treated layer, however, no crack is observed in the vicinity of the dense layer. This is attributed to the stress relaxation because of the self-annealing effect of the initially formed laser-scanned tracks. In the second region, the feathery-like structures and fine dendrites are formed. The nitrogen diffusion is responsible for the formation of Fe_4N reach feathery-like structure in this region. Ferritic and austenite transformation into martensite takes place in this region due to high cooling rates. In the third region, cellular structures are formed because of relatively slower cooling rates as compared to that corresponding to the surface region. The cellular structures are deformed in irregular shapes in the fourth region where the heat-affected zone is started to form. The method adopted in the present study for the laser surface treatment of pre-prepared high-speed tool steel has a significant potential to be implemented in the tool industry. This is due to the formation of the homogeneous structures at the treated surface with precision operation, shallow heat-affected zone, and low cost.

Acknowledgement

The authors acknowledge the support of King Fahd University of Petroleum and Minerals Dhahran, Saudi Arabia for this work.

References

[1] B.J. Abdul Aleem, M.S.J. Hashmi, B.S. Yilbas, Laser surface treatment of high speed steel: presence of TiC particles at the surface, *Surf. Interface Anal.* **2012**, *44*(2), 150-155.
[2] M. Bonek, L.A. Dobrzanski, E. Hajduczek, A. Klimpel, Effect of laser surface melting on structure and properties of a high speed tool steel. *J. of Materials Processing Technology* **2006**, *175*, 45-54.
[3] O. Verezub, Z. Kalazi, G. Buza, N.V. Verezub, G. Kaptay, Classification of laser beam induced surface engineering technologies and in situ synthesis of steel matrix surface nanocomposites, *Surf. Eng.* **2011**, *27*, 428-435.
[4] K.W. Guo, Effect of polishing parameters on morphology of DF2 (AISI-O 1) steel surface polished by Nd:YAG laser, *Surf. Eng.* **2009**, *25*, 187-195.
[5] S.M. Shariff, T.K. Pal, G. Padmanabham, S.V. Joshi, Sliding wear behaviour of laser surface modified pearlitic rail steel, *Surf. Eng.* **2010**, *26*, 199-208.
[6] A.R. Shankar, U.K. Mudali, Laser surface modification of plasma sprayed yttria stabilised zirconia coatings on type 316 L stainless steel, *Surf. Eng.* **2009**, *25*, 241-248.
[7] R.F. Li, Z. G. Li, J. Huang, Y.Y. Zhu, Microstructure and wear properties of laser processed Ni based amorphous matrix coatings, *Surf. Eng.* **2012**, *28*, 513-516.
[8] J.C. Betts, B.L. Mordike and M. Grech, Characterisation, wear and corrosion testing of laser-deposited AISI 316 reinforced with ceramic particles, *Surf. Eng.* **2010**, *26*, 21-29.
[9] Q.J. Zhu, X.H. Wang, S.Y. Qu, Z.D. Zou, Microstructure and wear properties of laser clad Fe based amorphous composite coatings, *Surf. Eng.* **2009**, *25*, 201-205.

[10] B.S. Yilbas, S.S. Akhtar, Karatas C., Chatwin, Laser embedding of TiC particles into the surface of phosphor, *Surf. Interface Anal.* **2012**, *44*(7), 831-836, 11.

[11] B.S. Yilbas, S.S. Akhtar, Karatas C., Laser gas-assisted processing of carbon coated and TiC embedded Ti-6Al-4 V alloy surface, *Appl. Surf. Sci.* **2010**, *257*(2), 531-537.

[12] B.S. Yilbas, N. Al-Aqeeli, C. Karatas, Laser control melting of alumina surfaces with presence of B4C particles, *J. Alloys Compd.*, **2012**, *539*, 12-16.

[13] Z.A. Khana, M. Hadfield, S. Tobe, Y. Wang, **2005**, Ceramic rolling elements with ring crack defects - a residual stress approach, *Mater. Sci. Eng. A*, *404*, 221–226.